Multi-time scale control of Southern Ocean diapycnal mixing over Atlantic tracer budgets

Elizabeth Ellison[1] · Laura Cimoli[2] · Ali Mashayek[1]

Abstract

Oceanic cross-density (diapycnal) mixing helps sustain the ocean density stratification and its Meridional Overturning Circulation (MOC) and is key to global tracer distributions. The Southern Ocean (SO) is a key region where different overturning cells connect, allowing nutrient and carbon rich Indian and Pacific deep waters, and oxygen rich Atlantic deep waters to resurface. The SO is also rife with intense diapycnal mixing due to the interaction of energetic eddies and currents with rough topography. SO diapycnal mixing is believed to be of secondary importance for the MOC. Here we show that changes to SO mixing can cause significant alterations to biogeochemical tracer distributions over short and long time scales in an idealized model of the AMOC (Atlantic MOC). While such alterations are dominated by the direct impact of changes in diapycnal mixing on tracer fluxes on annual to decadal time scales, on centennial time scales they are dominated by the mixing-induced variations in the advective transport of the tracers by the AMOC. This work suggests that an accurate representation of spatio-temporally variable local and non-local mixing processes in the SO is essential for climate models' ability to (i) simulate the global biogeochemical cycles and air sea carbon fluxes on decadal time scales, (ii) represent the indirect impact of mixing-induced changes to AMOC on biogeochemical cycles on longer time scales.

Keywords Southern Ocean · Turbulent mixing · Carbon cycle · Tracer budgets

1 Introduction

In the ocean interior and away from boundaries, internal waves are mainly radiated by winds at the surface and by tidal and deep geostrophic flows interacting with rough bottom topography (MacKinnon et al. 2017). Breaking of internal waves induces turbulent mixing across density surfaces (i.e. diapycnally), which modifies water mass properties, and contributes to sustaining the deep branches of the global Meridional Overturning Circulation (MOC). Mixing is also key to the redistribution of heat, carbon, biological nutrients, and other tracers globally and in depth (Munk and Wunsch 1998; Law et al. 2003; Wunsch and Ferrari 2004; Watson and Naveira Garabato 2006). Ocean circulation models do not resolve the processes responsible for diapycnal mixing and parameterize diapycnal mixing in terms of a turbulent effective diffusivity, $\mathcal{K}$ (Large et al. 1994; Mashayek et al. 2015; Cessi 2019; Saenko et al. 2022).

1.1 Southern Ocean dynamics

Unbounded by continents, the Southern Ocean (SO) is a crucial link between waters formed in different ocean basins, and inter-basin exchanges of heat, carbon, nutrients and other tracers (Talley 2013). The lack of boundaries generates unique regional dynamics by allowing the formation of the Antarctic Circumpolar Current (ACC), an uninterrupted deep-reaching eastward flow driven by strong westerly winds. Within the ACC and in the upper ocean, the wind-driven Ekman transport is balanced by the resurfacing of deep waters. The Ekman transport is northward within the latitude band of the westerly winds, but southward towards Antarctica where easterly winds blow. In the deep SO, the

✉ Elizabeth Ellison
 e.ellison18@imperial.ac.uk

  Laura Cimoli
  lcimoli@ucsd.edu

  Ali Mashayek
  mashayek@imperial.ac.uk

[1] Imperial College, London, UK

[2] Scripps Institution of Oceanography, University of California, San Diego, USA

Fig. 1 A schematic of the Atlantic ocean circulation with an emphasis on the SO dynamics, watermasses, and tracers. Inspired by diagrams from Lauderdale et al. (2013) and Talley (2013)
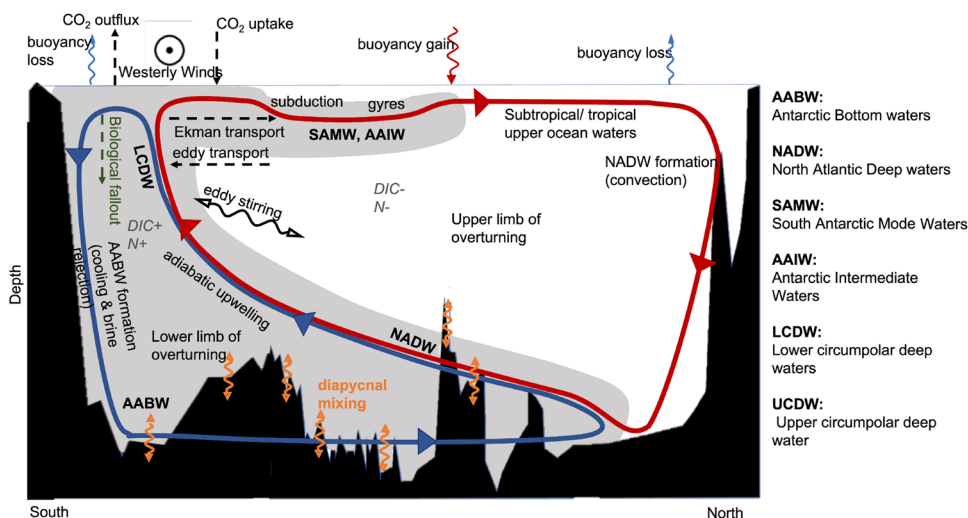
zonal pressure gradient sustained by deep topography allows for northward transport of the abyssal waters that form and sink around Antarctica (Marshall and Radko 2003; Ito and Marshall 2008; Tamsitt et al. 2017). While the Ekman transport primarily induces isopycnal (i.e. along density surfaces) water transports, in the SO interior diapycnal mixing allows for further vertical transport of waters and tracers (Garabato et al. 2007; Watson et al. 2013; Mashayek et al. 2017), see Fig. 1.

Within the SO, deep waters are upwelled adiabatically (i.e. along isopycnals) and are modified by surface buoyancy forcing upon turbulent entrainment into the mixed layer (Thompson et al. 2007; Ruan et al. 2017). Indian and Pacific deep waters predominantly upwell into a region of buoyancy gain and form the northward-flowing Antarctic Intermediate Water (AAIW) and South Antarctic Mode Water (SAMW) (Marshall and Speer 2012; Ruan et al. 2017). These waters eventually return to the SO as North Atlantic Deep Waters (NADW), completing the *upper* Atlantic MOC cell (AMOC; Red arrows in Fig. 1). Alternatively, waters can upwell into a region of buoyancy loss in the SO, as happens for up to 75% of the NADW, forming the denser Antarctic Bottom Waters (AABW) (Sloyan and Rintoul 2001; Marinov et al. 2008; Marshall and Speer 2012; Talley 2013; Silvester et al. 2014; Ruan et al. 2017). These abyssal waters sink and move northward along topographic ridges and canyons, and are then converted to deep waters through diapycnal mixing above the rough seafloor (Ito and Marshall 2008; De Lavergne et al. 2016) (Orange arrows in Fig. 1), forming the *lower* AMOC cell (Blue arrows in Fig. 1).

From direct observational estimates, inverse bulk budgets, and numerical models, the SO is known to have strong regional variations in diapycnal mixing rates, with values ranging from 10^{-5} m^2 s^{-1} to as high as 10^{-3} m^2 s^{-1} (Naveira Garabato et al. 2004; Ledwell et al. 2011; St. Laurent et al. 2012; Watson et al. 2013; Mashayek et al. 2017; Naveira

Garabato et al. 2019). This mixing is generated by strong ACC bottom currents interacting with rough topography, causing intense turbulence over abyssal ridges, mountains and rises (Naveira Garabato et al. 2004; Nikurashin and Ferrari 2013; Ferrari 2014) (Orange arrows in Fig. 1).

1.2 Southern Ocean biogeochemistry

65% of interior ocean waters make first contact with the atmosphere in the SO (Palter et al. 2010; DeVries and Primeau 2011), with Pacific and Indian deep waters bringing waters rich in dissolved inorganic carbon (DIC) and nutrients to the surface (Marinov et al. 2008). Thus, the SO connects the vast reservoir of nutrients and carbon below the mixed layer with the surface (Marshall and Speer 2012) (DIC$^+$ and N$^+$ grey waters in Fig. 1). Vigorous vertical diapycnal mixing also enhances the supply of nutrients from the deep ocean to the surface (Palter et al. 2010). Globally, the supply of surface nutrients is dominated by their upwelling in the SO (Palter et al. 2010; Moore et al. 2013). Patterns of SO circulation are therefore key to controlling global biogeochemical cycles, the exchange of carbon dioxide (CO$_2$) between the atmosphere and the deep ocean, and the response of the ocean and atmosphere to climate change (Sarmiento et al. 2004; Klocker 2018). The upwelling branch of the MOC is especially key to controlling the global climate from both dynamical and biochemical perspectives (Marshall and Speer 2012).

The global distribution of conservative and non-conservative tracers is sensitive to ocean circulation and ventilation (Doney et al. 2004; Gnanadesikan et al. 2004; Talley et al. 2016). Enhanced SO diapycnal mixing is known to alter tracer distributions through increased deep ocean ventilation of intermediate waters in the SO, reducing ocean carbon storage through the biological and solubility carbon pumps (Gnanadesikan et al. 2004; Marinov et al. 2008; Marinov

and Gnanadesikan 2011). Such changes are believed to be due to the interior diapycnal mixing altering the MOC over centennial to millennial time scales.

Theoretical studies have highlighted that diapycnal mixing rates in the deep SO are not of leading-order importance for regulating the global MOC, and are secondary to the role of winds, eddies, and surface buoyancy forcing. However, mixing in the ocean basins to the north of the SO plays a primary role in regulating the ocean circulation, and closes the MOC by upwelling the abyssal waters that form and sink at high latitudes (Ito and Marshall 2008; Nikurashin and Vallis 2011; Wolff et al. 2011; Nikurashin and Vallis 2012; Mashayek et al. 2015). Limited work has been carried out to assess the sensitivity of global biogeochemical tracer distributions to SO diapycnal mixing rates.

In this work, we examine (i) the role of diapycnal mixing in the SO on Atlantic tracer budgets over varying time scales, using an idealised single-basin model, and (ii) whether these changes are due to altered tracer diffusion or changes to the ocean circulation. We show that diapycnal mixing in the SO is crucial in setting the distribution of tracers on a range of time scales through two mechanisms. On centennial time scales, circulation and tracer advection changes dominate, especially when looking at distribution changes on a global scale, whereas changes to tracer diffusion dominate over annual to decadal time scales, especially within the SO region.

2 Model description

This work uses the zonally-averaged model of the AMOC by Nikurashin and Vallis (2012) (hereafter NV12), extended in Watson et al. (2015) to include a simple biochemical model based on that introduced in Ito and Follows (2005). The model, and similar ones, have been used extensively over the past decade to study various aspects of the role of the MOC in the climate system from both dynamical and biochemical aspects (e.g. Mashayek et al. 2013; Stewart et al. 2014; Ferrari et al. 2014; Watson et al. 2015; Jansen and Nadeau 2016). Thus, we simply provide a brief phenomenological description of the model here and refer the reader to the original works for more details.

2.1 The physical model

In the NV12 model, the Atlantic Ocean is split into three key areas: a SO circumpolar channel, a North Atlantic deep water formation zone, and the ocean mid-latitude basin that connects the two (consistent with the schematic in Fig. 1). While NV12 employed a constant $\mathcal{K}$ value throughout the water column in all three zones, here we consider vertically variable mixing and distinguish between the mixing in the

mid-latitude basin from that in the SO. Here, we study the sensitivity of tracer distributions to variations in SO diapycnal mixing.

2.2 The biochemical model

The simple biochemical component that was added to NV12 in Watson et al. (2015) allows for the representation of the coupled evolution of nutrients (N) and carbon (C), where N represents the ultimate limiting nutrient phosphate. Organic material is parameterized to sink downward, measured in units of phosphate, with the biological export time scale set to 360 days. A well-mixed atmospheric box is coupled to the ocean carbon cycle such that the partitioning of C between the atmosphere and the ocean is explicitly calculated in the model. The model conserves the total amount of C in the atmosphere and the ocean; if C is gained in the ocean, it must be lost in the atmosphere.

The biochemical tracers (C, N) are transported by advection and diffusion and have sources and sinks via biological activity (F_p) of uptake and remineralization. The concentration of C is able to change via surface fluxes driven by pCO_2 differences to account for air-sea gas transfer. More explicitly, the equations for C and N are

$$\partial_t N + J(\psi, N) = \partial_z(\mathcal{K}\partial_z N) + \partial_z F_p, \tag{1}$$

$$\partial_t C + J(\psi, C) = \partial_z(\mathcal{K}\partial_z C) + R\partial_z F_p + C_{flux}\|_{z=0}, \tag{2}$$

$$\begin{aligned} C_{flux} = &-(k_w \times k_H) \times (pCO_2 a - pCO_2 o) \\ &\times (1 - \text{ice cover}), \end{aligned} \tag{3}$$

where ψ is the meridional overturning streamfunction representing the AMOC (Figs. 1, 3a, b), k_w is the air-sea CO_2 exchange constant and k_H is the fugacity of CO_2, pCO_2a is the partial pressure of CO_2 in the atmosphere, and pCO_2o is the partial pressure of CO_2 in the surface ocean, all as in Watson et al. (2015). The second term on the left hand side represents advection of N and C by the AMOC, the first term on the right hand side represents turbulence diapycnal mixing, and the final term represents biological activity (Ito and Follows 2005). Biological activity in surface waters removes both N and C at the ratio set by R, with N and C both released by respiration as organic matter sinks.

2.3 Experiment design

Our goal is to explore the sensitivity of the AMOC and tracer budgets to SO mixing. Figure 2a shows the diapycnal mixing, $\mathcal{K}$, in the deep Atlantic region based on the sum of the tidal mixing estimates of de Lavergne et al. (2020) and the lee wave mixing estimates of Nikurashin and Ferrari
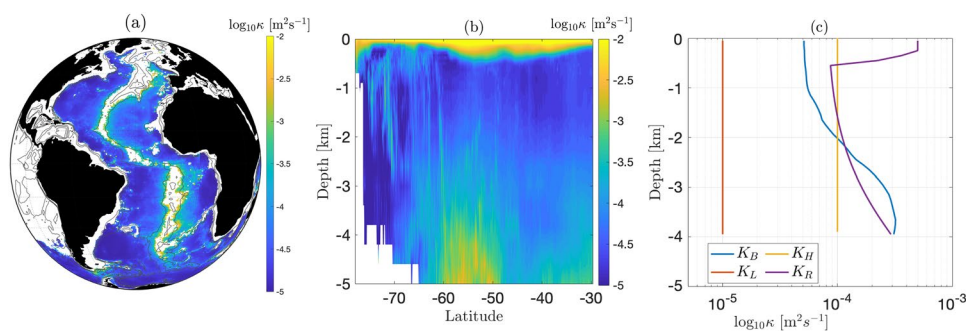
Fig. 2 **a** Turbulent diffusivity in the deep Atlantic basin (3000 m) based on the tidal mixing estimate of de Lavergne et al. (2020) and lee-wave mixing estimate of Nikurashin and Ferrari (2013). **b** Zonally-averaged diapycnal mixing in the SO from a combination of the interior mixing shown in panel *a* and wind-induced surface mixing based on the Southern Ocean Estate Estimate (SOSE; Verdy and Mazloff (2017)). **c** Basin-averaged diffusivities employed in the model: $\mathcal{K}_B$ is prescribed in the mid-latitude basin (and held the same in all experiments) whereas $\mathcal{K}_R$, $\mathcal{K}_L$, and $\mathcal{K}_H$ are employed in the SO for various perturbations. $\mathcal{K}_B$ is averaged over the mid-latitude basin (32°S to 48°N) based on the estimate in panel **a**. $\mathcal{K}_R$ is the SO-averaged diffusivity based on the estimate in panel **b**. $\mathcal{K}_L$ and $\mathcal{K}_H$ are the two canonical values representing the lower and upper bounds of ocean interior mixing. $\mathcal{K}_L = 10^{-5}$ m^2/s and $\mathcal{K}_H$2 10^{-4} m^2/s

(2013). Figure 2b shows the global zonally-averaged diapycnal mixing in the SO from a combination of tides and lee waves with the addition of mixed-layer mixing from the observationally-constrained Southern Ocean Estate Estimate Verdy and Mazloff (2017).

In all experiments (soon to be introduced), the mixing in the mid-latitude basin will be fixed to an average of the above-mentioned map (i.e. from tides plus lee waves) shown by the blue curve in Fig. 2c ($\mathcal{K}_B$). All surface forcings are kept constant in all experiments, and are as prescribed in NV12 (Nikurashin and Vallis 2012). In the SO, we consider three paradigms: the Low mixing scenario of $\mathcal{K}_\mathcal{L} = 10^{-5}$ m^2/s, the High mixing scenario of $\mathcal{K}_\mathcal{H} = 10^{-4}$ m^2/s, and the Realistic mixing scenario motivated by Fig. 2b, referred to as $\mathcal{K}_R$. It should be noted that 10^{-5} and 10^{-4} m^2/s are canonical values in physical oceanography, respectively representing the background mixing in the ocean and the mixing required for closure of the MOC (Munk 1966; Munk and Wunsch 1998; Waterhouse et al. 2014; Ferrari et al. 2014). The sharp transition between the mixing profiles across the interface of the SO channel and the mid-latitude basin reflects the difference in turbulence regimes in the two regions in the real world. While tidal mixing is dominant in the mid-latitude basin to the north, lee waves (excited by the interaction of the ACC and its overlying eddies with rough topography) dominate interior mixing in the SO (e.g. see Fig. 1 in Nikurashin and Ferrari (2013) and Fig. 2b here).

Since $\mathcal{K}_B$ will be fixed in all experiments, hereafter we will use $\mathcal{K}_R$, $\mathcal{K}_L$, and $\mathcal{K}_H$ to name the experiments. While in some cases the same SO diffusivity will be applied to density, N, and C, in others we will apply a mixing profile to N and C that is different from that applied to density. This will distinguish between the direct impact of mixing on tracers from the indirect effect on tracers because of the changes to the AMOC induced by the mixing of density. Thus, in naming experiments we will use superscripts 't' and 'ρ' to refer to tracer and density mixing. For example, an experiment named $[\mathcal{K}_H^t, \mathcal{K}_L^\rho]$ refers to one in which high SO mixing acts on tracers while low SO mixing acts on density, whereas $\mathcal{K}_L$ simply refers to an experiment in which low SO mixing is applied to both tracers and density.

The $\mathcal{K}_L$ experiment, hereafter referred to as the 'control', is run until an equilibrated overturning circulation is achieved (4000 yrs) and then extended until the ocean biochemistry reaches an equilibrated state as well (another 4000 yrs). C and N are initialized with uniform concentrations (2.2e^{-3} mol N m^{-3} and 2.2 mol C m^{-3} respectively (Watson et al. 2015)). The atmospheric carbon concentration is set to 278 part per million (ppm), representative of the pre-industrial level (Ito and Follows 2005). Starting from this equilibrated $\mathcal{K}_L$ solution, we run a host of configurations varying the SO density and tracer diffusivities. Each run is 4000 yrs long so that a new equilibrium is achieved. In this work we examine changes to both transient model solutions and the equilibrated changes for each experiment.

2.4 Model verification

Figure 3a–c compares the model solution for the control case to the circulation inferred from a climatologically-constrained ocean state estimate (ECCO Forget et al. (2015)). In the control run ($\mathcal{K}_L$), the upper cell extends to ~2000 m deep with a maximum strength of 17 Sv while the lower cell transport is about 4 Sv (Fig. 3b), both well within the range of inverse models (Lumpkin and Speer 2007; Talley 2013) and ocean state estimates (Forget et al. 2015; Cessi 2019). Panel *c* compares the model stratification in the Atlantic (for experiments $\mathcal{K}_L$, $\mathcal{K}_H$, $\mathcal{K}_R$) with the Atlantic World Ocean Circulation Experiment climatology (WOCE Gouretski and Koltermann (2004)). Since the Atlantic mid-latitude basin
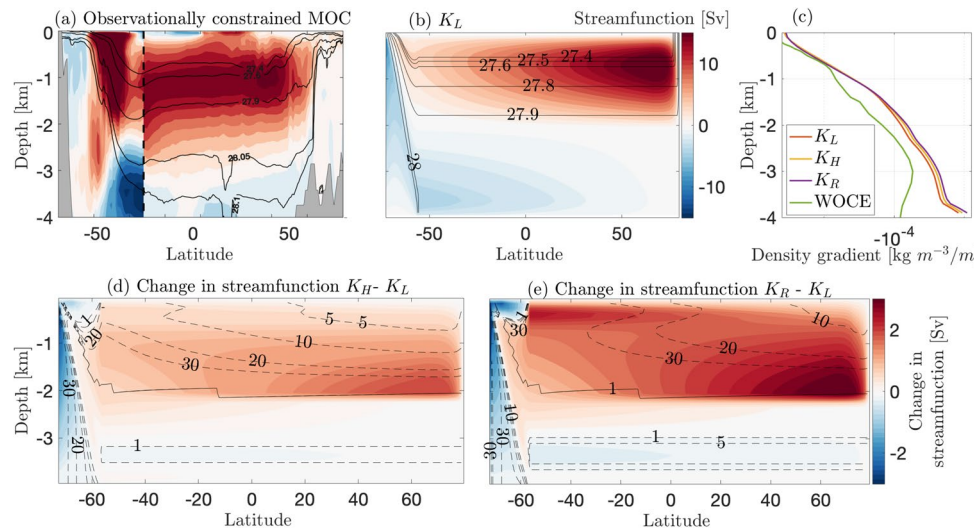
Fig. 3 a Zonally-averaged AMOC streamfunction (ψ in Eqs. 1,2) from a climatologically-constrained ocean estimate (ECCO; Forget et al. (2015)). Each Sverdrup (Sv)=10^6 m^3/s. The streamfunction is calculated in the Atlantic basin up to 32°S and globally between 70-32°S. Neutral density contours are in black. **b** The overturning streamfunction for the control case ($\mathcal{K}_L$) with density contours overlain (black lines). **c** Vertical gradient of neutral density (Jackett and McDougall 1997) in the model mid-latitude basin for $\mathcal{K}_L$ (red), $\mathcal{K}_H$ (yellow), and $\mathcal{K}_R$ (purple), compared to density gradient from World Ocean circulation Experiment (WOCE Gouretski and Koltermann (2004)) climatology averaged between 48°N to 32°S in the Atlantic basin (green). **d** Change in overturning circulation between $\mathcal{K}_H$ and $\mathcal{K}_L$ experiments. Dashed lines indicate percentage change in overturning streamfunction from $\mathcal{K}_L$. **e** Similar to **d** but for the difference between $\mathcal{K}_R$ and $\mathcal{K}_L$

diffusivity is fixed at $\mathcal{K}_B$ for all experiments, unsurprisingly the model stratification is similar in all three experiments. This implies the secondary influence of the SO mixing on the mid-latitude basin stratification, consistent with theoretical arguments discussed earlier (Nikurashin and Vallis 2012). The model stratification is in reasonable agreement (given its idealized nature) with climatology in the upper 3 km. This agreement suffices for our purposes, since our primary focus is on the upper AMOC cell and the southward flowing limb of the upper cell (or in other words, on isopycnals that outcrop in both polar regions). The disagreement in stratification in the abyssal ocean has implications on millennial time scales on which the single-basin nature of our analysis most likely introduces larger errors. Nevertheless, for our primary messages and the time scales of concern, the model stratification and the AMOC rate of overturning cells are adequate.

Altered SO mixing causes up to a 30% change in the strength of circulation (Fig. 3d, e) after 4000 years. Increasing SO mixing to $\mathcal{K}_H$ and $\mathcal{K}_R$ increases AMOC strength by up to ~3 Sv in the upper branch and by ~2 Sv in the deep branch. The maximum transport is increased from 16.9 Sv in $\mathcal{K}_L$, to 17.8 Sv in $\mathcal{K}_H$, and to 18.8 Sv in $\mathcal{K}_R$. Previous studies also found increased strength of convection with higher SO vertical mixing (Marinov et al. 2008). The upper cell is also deepened with enhanced mixing, as in Gnanadesikan (1999), Nikurashin and Vallis (2012), as the increased downward

mixing of buoyant surface waters in the SO deepens the pycnocline, altering the structure of the AMOC. As we will show, this change is effective on time scales of equilibration of the circulation (centennial to millennial). We will also show that the direct impact of mixing on tracers can be more significant and effective on shorter time scales.

The distribution of C and N produced by the model are also qualitatively similar to observations and reproduce many of the key features (Fig. 4). The surface waters are nutrient depleted due to phytoplankton productivity, even if the model lacks the upper ocean gyre-induced circulation and thus does not capture the observed deeper nutrient and CO_2 minimum. As mentioned before, this study focuses on the inter-hemispheric isopycnals that outcrop in both the northern and southern high-latitudes and lay below the upper ocean gyre circulation. As waters circulate and organic matter sinks, the N and C concentrations in old deep waters get enhanced (Fig 1). The short residence time of these waters in the surface SO means that biota are unable to utilize all of the nutrients (Ito and Follows 2005). Therefore, AABW and AAIW have high (preformed) N content. The concentration of nutrients in AAIW are rapidly depleted as waters travel north due to productivity. Regions with high (low) N levels also have high (low) C concentrations, as photosynthesis takes in both, and remineralisation releases both.

Fig. 4 Concentration of N from experiment $\mathcal{K}_L$, compared to the climatological zonally-integrated phosphate in the Atlantic basin from WOCE (Gouretski and Koltermann 2004) in **b**. Concentration of C from experiment $\mathcal{K}_L$ in **c** is also compared to the climatological zonally-integrated C from the Global Ocean Data Analysis Project (GLODAP Olsen et al. 2019) in **d**
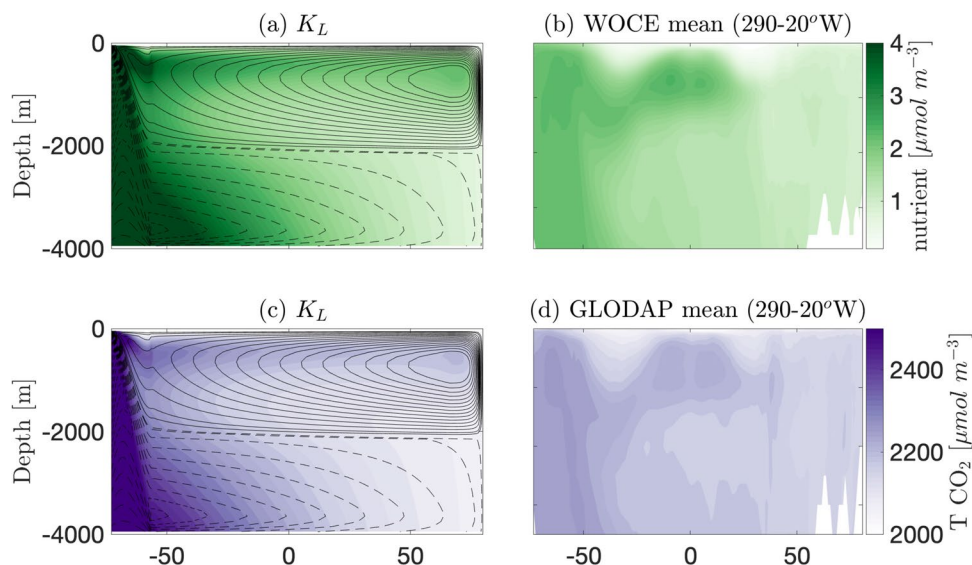
3 Results: sensitivity of C & N distribution to Southern Ocean mixing

3.1 Multiscale temporal changes

Figure 5 shows the N distribution anomaly between various mixing scenarios and the control simulation ($\mathcal{K}_L$), over the first 100 years after mixing in the SO is perturbed for C & N and/or density. The first row shows the total change for $\mathcal{K}_H$, when both $\mathcal{K}^t$ (which acts on N and C) and $\mathcal{K}^\rho$ (which acts on density) are enhanced. The net change is due to two contributions: (I) the indirect impact caused by alterations to the density field (higher $\mathcal{K}^\rho$) changing the AMOC, and (II) the direct impact of enhanced $\mathcal{K}^t$ directly on the C & N gradient.

The indirect impact is isolated in the second row where $\mathcal{K}^t$ is unchanged from the control but $\mathcal{K}^\rho$ is enhanced. The anomaly is large north of the SO channel, reflecting the change in the AMOC due to the modification of the Atlantic density stratification thanks to enhanced SO density mixing.

The direct impact is isolated in the third row where $\mathcal{K}^\rho$ is unchanged from the control, but $\mathcal{K}^t$ is enhanced. This anomaly is expectedly SO-focused and evolves much faster than the former signal in the second row. Very minimal changes are seen north of the SO channel.

The last row bears similarity to the first row as it too captures the impact of enhanced mixing (on both C & N and density) using a more realistic mixing profile $\mathcal{K}_R$ than the simple $\mathcal{K}_H = 10^{-4}$ m²/s. The SO change is more dramatic for the realistic mixing profile, since it mimics the large surface turbulent mixing induced by the SO storm tracks (Fig. 2c). The higher $\mathcal{K}^t$ rates in the first, third, and fourth rows disperse the C & N more rapidly from C & N-rich regions such as the AAIW and lower cell waters. C & N are lost from SO upper AAIW waters, and mixed into the C & N depleted

regions above and below. Such changes are the greatest in $\mathcal{K}_R$, showing the importance of the enhanced surface water mixing rates.

To further quantify the changes to SO and mid-latitude basin N inventories by mixing perturbations, we calculate the mean absolute changes between various experiments and the control run ($\mathcal{K}_L$). The results are shown in Fig. 6 and are broken down into SO and the mid-latitude basin as well as into upper ocean versus full depth. Since the results based on $\mathcal{K}_R$ are similar to those experiments with $\mathcal{K}_H$, we don't include the former in this figure to avoid overcrowding.

The mean differences in N concentrations between various experiments and the control run ($\mathcal{K}_L$) increase over the 4000 years of experiments in all regions of the Atlantic. The changes to N concentrations in the surface waters of $\mathcal{K}_H$ show the greatest changes at all times, changing by a mean of 20% once a new steady-state is reached (Fig. 6 solid red line). The SO shows initially higher changes in N distributions than the Atlantic (blue vs black lines). By 500 years, however, changes to N distributions in the mid-latitude Atlantic basin and the SO are comparable at around 7%. This emphasizes the global impact of altered SO diapycnal mixing on N distributions.

Over the first 5 years, changes to N distributions are only felt in the interior SO and SO + mid-latitude basin surface waters in experiments where $\mathcal{K}^t$ is enhanced (solid and dotted red and blue lines). It takes over 100 years for the enhanced $\mathcal{K}^t$ in the SO to have an impact on the distribution of N in the Atlantic basin, and even on millennial time scales, this change is less than 2% (dotted green and black lines). By ~5 years, enhanced $\mathcal{K}^\rho$ alters N distributions in just the SO, but only by 1%, while changes to $\mathcal{K}^t$ alter the N distributions by 4% in the same region (dashed vs dotted blue lines). It takes 20 years for alterations to the AMOC to

Fig. 5 Change in N concentration at t=5, 50 and 100 years from the N concentration for the $\mathcal{K}_L$ experiment in steady-state, as was shown in Fig. 4a. First Row: change between $\mathcal{K}_H$ and $\mathcal{K}_L$ experiments. Second Row: between $[\mathcal{K}_L^t, \mathcal{K}_H^\rho]$ and $\mathcal{K}_L$ experiments. Third row: between $[\mathcal{K}_L^t, \mathcal{K}_H^\rho]$ and $\mathcal{K}_L$ experiments. Fourth row: between $\mathcal{K}_R$ and $\mathcal{K}_L$ experiments. Red/blue implies increased/decreased tracer concentration. Black overlain lines indicate zonally averaged residual overturning circulation for each experiment, with labels indicating streamfunction in Sv
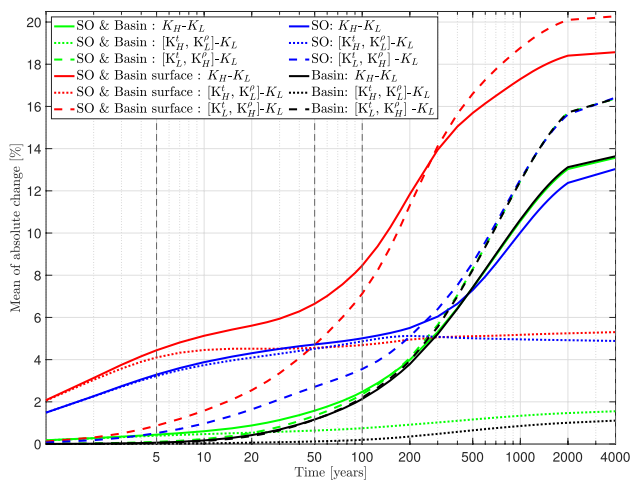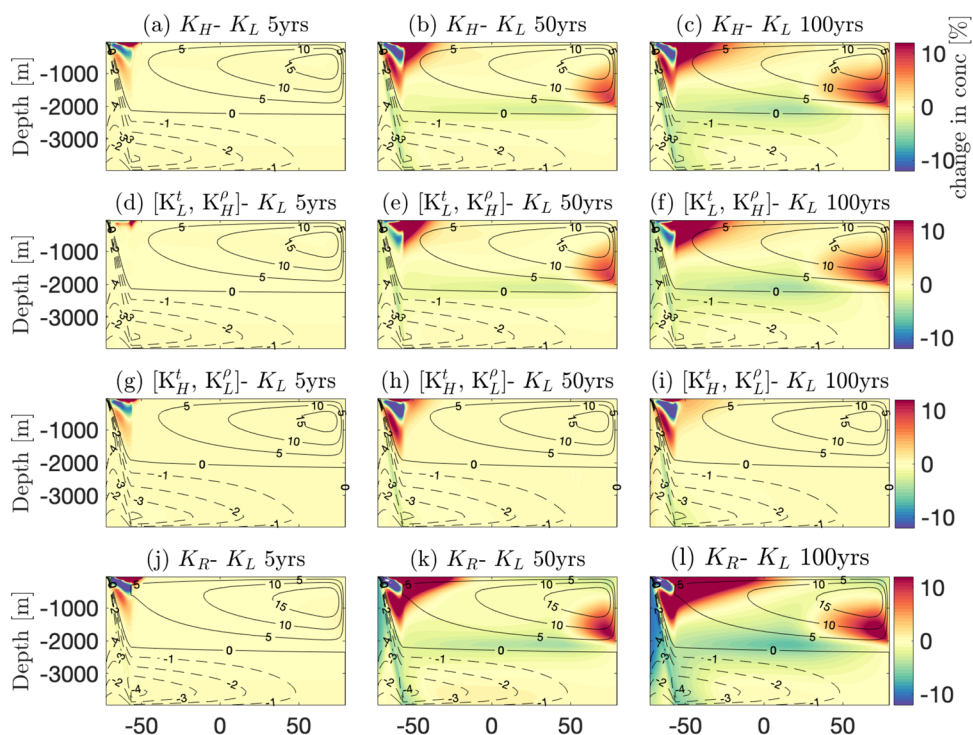
Fig. 6 Mean of absolute change in integrated N concentration for various inventories: the entire ocean (SO+mid-latitude basin) in green, the surface ocean (top 200m of SO+mid-latitude basin) in red, only the mid-latitude basin (full depth) in black, and only the SO (full depth) in blue. Solid lines denote the difference between $\mathcal{K}_H$ and $\mathcal{K}_L$ experiments, dotted lines represent differences between $[\mathcal{K}_H^t, \mathcal{K}_L^\rho]$ and $\mathcal{K}_L$ experiments, and dashed lines denote differences between $[\mathcal{K}_L^t, \mathcal{K}_H^\rho]$ and $\mathcal{K}_L$ experiments. Vertical dashed lines indicate the time slices considered in Fig. 5

alter the N distributions in the mid-latitude basin. Changes to N distributions in the mid-latitude basin are always greater for enhanced $\mathcal{K}^\rho$ as compared to cases with $\mathcal{K}^t$. In the SO, it takes at least 200 years for the indirect effect of altered

AMOC to alter tracer distributions more significantly than just increasing $\mathcal{K}^t$ (dashed vs dotted blue lines).

We also carried out a similar analysis for passive tracers, released with initial distributions similar to that of the N distribution in the $\mathcal{K}_L$ experiment. The results, which are not discussed here, looked qualitatively similar to what was described above for N, albeit with lower magnitudes in the concentration anomalies due to the lack of biological processes.

3.2 Long-term equilibrated changes

Mixing is spatio-temporally variable, and so a steady-state solution does not necessarily describe the real world. However, it is insightful to consider the long-term equilibrated solutions of the perturbation experiments to gain an understanding of the order of magnitude importance of the changes. In Fig. 7 we plot the changes in the steady-state C and N distributions between the various experiments and the control experiment. In all cases, the C and N concentrations are increased in surface waters, as found previously with enhanced SO deep water upwelling (Marinov et al. 2008). Changes to N are overall more prominent than those to C, as shown by the percentage change contours of Fig. 7. The greatest changes for both occur in the $\mathcal{K}_R$ experiment, highlighting the conservative nature of our choice of high diffusivity in $\mathcal{K}_H$.

Consistent with the transient solutions, in experiments with enhanced mixing only acting on ρ (panels c,g), the
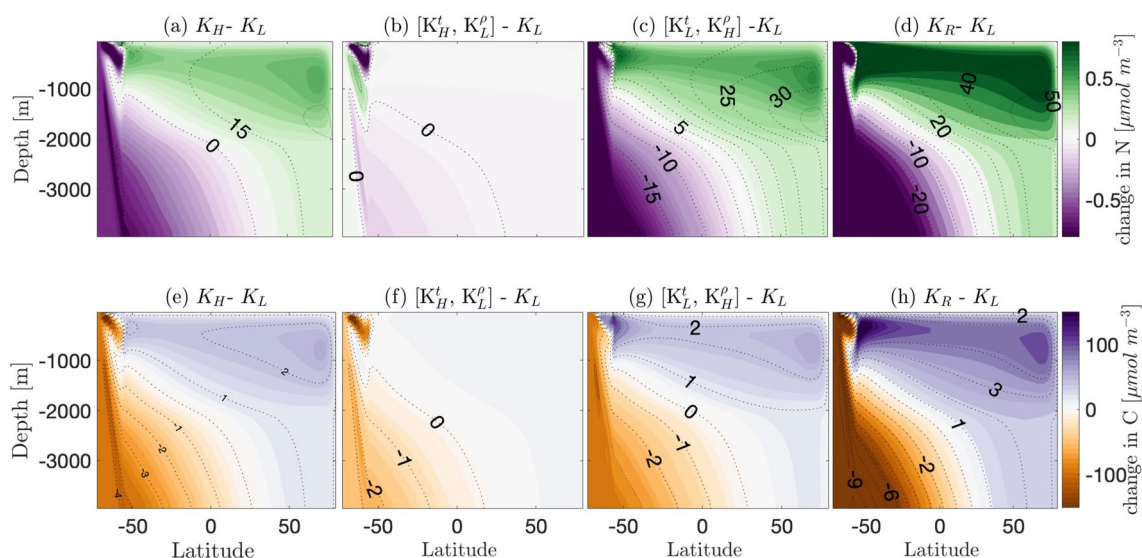
Fig. 7 Equilibrated changes to N and C distributions. Top row: change in N concentration between $\mathcal{K}_L$ and **a** $\mathcal{K}_H$, **b** $[\mathcal{K}_H^t, \mathcal{K}_L^\rho]$, **c** $[\mathcal{K}_L^t, \mathcal{K}_H^\rho]$, and **d** $\mathcal{K}_R$. Green/purple denotes regions of increased/decreased N concentration. Black-labelled overlain lines indicate percentage changes from $\mathcal{K}_L$. Bottom row: same as above but for C, with purple/orange denoting regions of increased/decreased C concentration

signal extends beyond the SO channel since it comes from changes to the whole AMOC. As a result, on the long-term (millennial) equilibration time scale, the indirect impact of mixing on tracers due to mixing-induced AMOC changes can overwhelm the direct impact of mixing on tracers. However, as was discussed in relation to Figs 5, 6, on inter-annual to decadal time scales, the direct impact is dominant and perhaps more readily relevant to the short time scale climate change.

Again consistent with the transient solutions, in the experiments with enhanced mixing only applied to $N\&C$, the signal is strongest in the SO due to the transfer of tracers from the $C\&N$ rich lower cell to the upper cell of the AMOC (panels b,f). The subsequent increase in the surface N concentration is significant for the uptake of C by biological productivity, and the sinking of organic matter containing C and N as part of the biological carbon pump. An increase in surface nutrient concentrations with enhanced SO upwelling has been observed previously (Marinov et al. 2008).

The climatic implications of the changes to N and C budgets may be encapsulated through the net change in atmospheric pCO$_2$ concentrations between the various experiments and the control run in which weak mixing acts on N, C, and ρ. This is summarized in Table 1. The direct impact of enhanced mixing on tracers, as in $[\mathcal{K}_H^t, \mathcal{K}_L^\rho]$, cause the redistribution of C to the upper surface waters. This is potentially important for atmospheric C concentrations. These surface waters allow C to be exchanged between the atmosphere and the ocean. Therefore, enhanced $\mathcal{K}^t$ results in only a very slight increase in C content of the AMOC upper cell, but an increase in atmospheric C reservoir of 12.3 ppm (Table 1).

On the other hand, although increased $\mathcal{K}^\rho$ caused a stronger redistribution of C within the AMOC upper cell, this C was not directed to the very surface waters. Therefore the redistribution was not as important for ocean-atmosphere fluxes of C, but caused more drastically observable changes to the C content of the upper cell. Enhanced $\mathcal{K}^t$ and $\mathcal{K}^\rho$ both cause a steady-state atmospheric CO$_2$ concentration greater than in $\mathcal{K}_L$, but the direct effect of the tracer mixing is stronger than the indirect effect of the density mixing (Table 1).

Of course, in the real ocean, the seasonality of mixed layer dynamics could be capable of inducing more entrainment of carbon-rich waters from below. To mimic this, our $\mathcal{K}_R$ experiment results in the greatest increase in atmospheric CO$_2$ content, due to the high surface mixing rates bringing carbon rich waters into contact with the atmosphere. The strong mixed layer mixing in the SO is known to raise predicted atmospheric CO$_2$ concentrations, and to make partitioning CO$_2$ into the deep ocean harder (Watson and Naveira Garabato 2006).

4 Discussion

This work highlights the sensitivity of tracer distributions (such as those of nutrients and carbon) in the global ocean to diapycnal mixing in the SO. The idealized nature of our model, and the mere consideration of a single ocean basin ('Atlantic'-like), imply that our results are not meant to represent the state of the real ocean. However, our primary two findings should transcend the idealism of our analysis setup. First, we showed that the enhanced mixing in the

SO exerts a significant control on the tracer budgets globally and well beyond the boundaries of the SO. Second, we showed that tracer responses to SO mixing manifest on two distinct time scales: one short (annual to decadal) due to the direct action of mixing on tracer gradients, and one long (centennial and longer) due to the indirect impact of mixing through changing the isopycnal slopes in the Southern Ocean, thereby altering the global deep stratification and the inter-hemispheric AMOC. We found both the direct and indirect impacts significant on their associated time scales.

Changes to nutrient concentrations within the SO occur on time scales of inter-annual to decadal, while the surface water nutrient concentrations begin to be modified by the change in the AMOC beyond 50 years. This time scale corresponds to the transport and utilization of nutrients by the northward SAMW (Palter et al. 2010) to be utilized for downstream productivity, as the resurfacing of deep nutrient rich waters at around 30°S ranges from multi-decadal to a centennial (Tamsitt et al. 2017). Given that between 30°S and 30°N upper ocean nutrient supply is dominated by waters originating in the SO, (Palter et al. 2010), the global nutrient and carbon budgets are therefore sensitive to SO mixing. Our results agree with the suggestion of Gnanadesikan et al. (2004) that, in a steady-state solution (i.e. on centennial to millennial timescales), tracer flux divergences are likely to be much smaller in comparison to changes to the advective fluxes of tracers, and that increasing the diapycnal mixing values in just the SO causes smaller changes to vertical diapycnal nutrient fluxes, and much larger changes to advection and convection.

The steady state atmospheric pCO_2 concentration was increased by ∼25 ppm when a 'realistic' mixing profile (within our idealized framework) is considered relative to a fixed diffusivity of $\mathcal{K} = 10^{-4}$ m²/s. Given that glacial-inter-glacial cycles in atmospheric pCO_2 were around 80 - 100 ppm (Sigman et al. 2010), and that present day to pre-industrial atmospheric carbon changes are around 130 ppm, this is a significant change, especially as this work was confined to just the Atlantic Ocean. This indicates the importance of accurate representation of turbulent mixing in surface waters of the SO in climate modelling.

Figure 8 summarizes our key messages by showing a zoomed in view of the zonally-averaged SO (from the model), and comparing the SO-branch of the upper and lower AMOC between the low mixing control run and the case with a realistic SO-averaged diffusivity. The background colour, from the control run, shows the richness of nutrients in the AABW within the SO. The arrows at mid-depths represent the interior mixing induced by the breaking of waves in the vigorous wave field of the SO which results in diapycnal diffusion of nutrients across density surfaces. It is the direct impact of enhancement to such mixing, which increases the rate of diapycnal upwelling of nutrients from
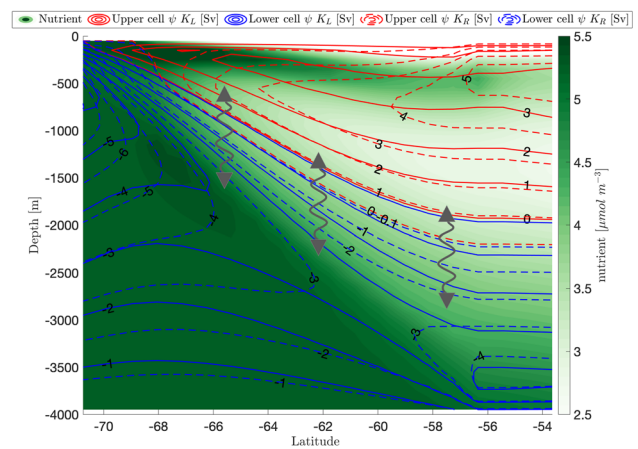
Fig. 8 Tracer distributions in the SO are altered via two processes: firstly, through the direct impact of mixing (grey arrows) on tracer gradients, and secondly by changing the SO density stratification and thereby the global AMOC. Red and Blue contours show the overturning stream functions for the upper and lower AMOC cells for the control $\mathcal{K}_L$ experiment (solid lines) vs the $\mathcal{K}_R$ experiment (dashed lines) in Sv. The background green colour represents the nutrient concentration from the equilibrated control experiment $\mathcal{K}_L$

Table 1 Change in steady state atmospheric pCO_2 from experiment $\mathcal{K}_L$

Experiment	Change in atmospheric pCO_2(ppm)
K_H	11.2
$[Kt_H, Kb_L]$	12.3
$[\mathcal{K}_L^t, \mathcal{K}_H^\rho]$	3.9
K_R	24.6

high concentration AABW into the nutrient poor water masses that introduces the largest changes in Atlantic *C* and *N* budgets, as well as in pCO_2 levels on decadal to centenial time scales. These water masses experience wind-driven upwelling along isopycnals at the boundary of the upper and lower cells within the ACC (see Fig. 1). On longer time scales, alterations to nutrient distributions arise from the change in AMOC structure from enhanced SO mixing. Such mixing changes the stratification within the SO, manifesting in the form of change to density layer slopes (Fig. 8 coloured contours). Given the global connectivity of the ocean basins through the SO, any change in SO isopycnal slopes translates to a change to the global deep stratification, thereby to alteration of the global AMOC. Full realization of such effects will require a multi-basin analysis.

Given that mixing is induced by turbulent events that are highly intermittent in time and space, this work highlights the inevitable need for realistic spatio-temporal representation of small scale SO mixing in climate models. In a recent complementary work, we reported a hyper-sensitivity of SO

air-sea carbon fluxes to moderate changes in upper ocean diapycnal mixing in a realistic ocean state estimate (Ellison et al. 2021). While that work was focused on the SO alone, as opposed to our Atlantic focus here, it shows that our idealized framework likely significantly underestimates the sensitivity of the global budgets to the SO mixing. Even with such underprediction, the changes reported herein are significant. While some parameterization of internal wave generation within the SO have been implemented in models previously, explicit parameterizations of small scale diapycnal mixing below the mixed layer in the SO are uncommon if not nonexistent.

Data Availability Data sharing not applicable to this article as no datasets were generated or analysed during the current study.

Declarations

Conflict of interest The authors have no conflict of interest to report.

References

Cessi P (2019) The global overturning circulation. Annu Rev Mar Sci 11:249–270

De Lavergne C, Madec G, Le Sommer J, Nurser AJG, Garabato ACN (2016) On the consumption of Antarctic Bottom Water in the abyssal ocean. J Phys Oceanogr 46(2):635–661. https://doi.org/10.1175/JPO-D-14-0201.1

de Lavergne C, Vic C, Madec G, Roquet F, Waterhouse AF, Whalen CB, Cuypers Y, Bouruet-Aubertot P, Ferron B, Hibiya T, Lavergne C, Vic C, Madec G, Roquet F, Waterhouse AF, Whalen CB, Cuypers Y, Bouruet-Aubertot P, Ferron B, Hibiya T (2020) A parameterization of local and remote tidal mixing. J Adv Model Earth Syst 12(5):2020–002065. https://doi.org/10.1029/2020MS002065

DeVries T, Primeau F (2011) Dynamically and observationally constrained estimates of water-mass distributions and ages in the global ocean. J Phys Oceanogr 41(12):2381–2401. https://doi.org/10.1175/JPO-D-10-05011.1

Doney SC, Lindsay K, Caldeira K, Campin JM, Drange H, Dutay JC, Follows M, Gao Y, Gnanadesikan A, Gruber N, Ishida A, Joos F, Madec G, Maier-Reimer E, Marshall JC, Matear RJ, Monfray P, Mouchet A, Najjar R, Orr JC, Plattner GK, Sarmiento J, Schlitzer R, Slater R, Totterdell IJ, Weirig MF, Yamanaka Y, Yool A (2004) Evaluating global ocean carbon models: the importance of realistic physics. Glob Biogeochem Cycles. https://doi.org/10.1029/2003GB002150

Ellison EC, Mashayek A, Mazloff MR (2021) Hypersensitivity of Southern Ocean air-sea carbon fluxes to turbulent diapycnal mixing. https://doi.org/10.1002/ESSOAR.10508126.1

Ferrari R (2014) Oceanography: what goes down must come up. Nature 513:179–180. https://doi.org/10.1038/513179a

Ferrari R, Jansen MF, Adkins JF, Burke A, Stewart AL, Thompson AF (2014) Antarctic sea ice control on ocean circulation in present and glacial climates. Proc Natl Acad Sci USA 111(24):8753–8758. https://doi.org/10.1073/pnas.1323922111

Forget G, Campin J-M, Heimbach P, Hill CN, Ponte RM, Wunsch C (2015) ECCO version 4: an integrated framework for non-linear inverse modeling and global ocean state estimation. Geosci Model Dev 8(10):3071–3104. https://doi.org/10.5194/gmd-8-3071-2015

Garabato ACN, Stevens DP, Watson AJ, Roether W (2007) Short-circuiting of the overturning circulation in the Antarctic Circumpolar Current. Nature 447(7141):194–197. https://doi.org/10.1038/nature05832

Gnanadesikan A (1999) A simple predictive model for the structure of the oceanic pycnocline. Science 283(5410):2077–2079. https://doi.org/10.1126/science.283.5410.2077

Gnanadesikan A, Dunne JP, Key RM, Matsumoto K, Sarmiento JL, Slater RD, Swathi PS (2004) Oceanic ventilation and biogeochemical cycling: understanding the physical mechanisms that produce realistic distributions of tracers and productivity. Global Biogeochem Cycles 18(4):1–17. https://doi.org/10.1029/2003GB002097

Gouretski V, Koltermann KP (2004) WOCE global hydrographic climatology. Berichte des BSH 35:1–52

Ito T, Marshall J (2008) Control of lower-limb overturning circulation in the Southern Ocean by diapycnal mixing and mesoscale eddy transfer. J Phys Oceanogr 38(12):2832–2845. https://doi.org/10.1175/2008JPO3878.1

Ito T, Follows MJ (2005) Preformed phosphate, soft tissue pump and atmospheric CO_2. J Mar Res. https://doi.org/10.1357/0022240054663231

Jackett DR, McDougall TJ (1997) A neutral density variable for the World's Oceans. J Phys Oceanogr 27(2):237–263. https://doi.org/10.1175/1520-0485(1997)027<0237:ANDVFT>2.0.CO;2

Jansen MF, Nadeau L-P (2016) The effect of southern Ocean surface buoyancy loss on the deep-ocean circulation and stratification. J Phys Oceanogr 46(11):3455–3470. https://doi.org/10.1175/jpo-d-16-0084.1

Klocker A (2018) Opening the window to the Southern Ocean: the role of jet dynamics. Sci Adv 4:eaao4710. https://doi.org/10.1126/sciadv.aao4719

Large WG, McWilliams JC, Doney SC (1994) Oceanic vertical mixing: a review and a model with a nonlocal boundary layer parameterization. Rev Geophys 32(4):363. https://doi.org/10.1029/94RG01872

Lauderdale JM, Naveira Garabato AC, Oliver KICC, Follows MJ, Williams RG, Garabato ACN, Oliver KICC, Follows MJ, Williams RG (2013) Wind-driven changes in Southern Ocean residual circulation, ocean carbon reservoirs and atmospheric CO_2. Clim Dyn1. https://doi.org/10.1007/s00382-012-1650-3

Law CS, Abraham ER, Watson AJ, Liddicoat MI (2003) Vertical eddy diffusion and nutrient supply to the surface mixed layer of the Antarctic Circumpolar Current. J Geophys Res C: Oceans. https://doi.org/10.1029/2002jc001604

Ledwell JR, St. Laurent LC, Girton JB, Toole JM, (2011) Diapycnal mixing in the Antarctic circumpolar current. J Phys Oceanogr 41(1):241–246. https://doi.org/10.1175/2010JPO4557.1

Lumpkin R, Speer K (2007) Global ocean meridional overturning. J Phys Oceanogr 37(10):2550–2562. https://doi.org/10.1175/JPO3130.1

MacKinnon JA, Zhao Z, Whalen CB, Waterhouse AF, Trossman DS, Sun OM, St. Laurent LC, Simmons HL, Polzin K, Pinkel R, Pickering A, Norton NJ, Nash JD, Musgrave R, Merchant LM, Melet AV, Mater B, Legg S, Large WG, Kunze E, Klymak JM, Jochum M, Jayne SR, Hallberg RW, Griffies SM, Diggs S, Danabasoglu G, Chassignet EP, Buijsman MC, Bryan FO, Briegleb BP, Barna A, Arbic BK, Ansong JK, Alford MH (2017) Climate process team on internal wave-driven ocean mixing. Bull Am Meteorol Soc 98(11):2429–2454. https://doi.org/10.1175/BAMS-D-16-0030.1

Marinov I, Gnanadesikan A, Sarmiento JL, Toggweiler JR, Follows M, Mignone BK (2008) Impact of oceanic circulation on biological carbon storage in the ocean and atmospheric pCO2. Glob Biogeochem Cycles 22:3. https://doi.org/10.1029/2007GB002958

Marinov I, Gnanadesikan A (2011) Changes in ocean circulation and carbon storage are decoupled from air-sea CO &lt;sub &gt;2 &lt;/sub &gt; fluxes. Biogeosciences 8(2):505–513. https://doi.org/10.5194/bg-8-505-2011

Marshall J, Radko T (2003) Residual-mean solutions for the Antarctic Circumpolar Current and its associated overturning circulation. J Phys Oceanogr 33:2341–2354. https://doi.org/10.1175/1520-0485(2003)033<2341:RSFTAC>2.0.CO;2

Marshall J, Speer K (2012) Closure of the meridional overturning circulation through Southern Ocean upwelling. https://doi.org/10.1038/ngeo1391, www.nature.com/naturegeoscience

Mashayek A, Ferrari R, Vettoretti G, Peltier WR (2013) The role of the geothermal heat flux in driving the abyssal ocean circulation. Geophys Res Lett 40(12):3144–3149. https://doi.org/10.1002/grl.50640

Mashayek A, Ferrari R, Nikurashin M, Peltier WR (2015) Influence of enhanced abyssal diapycnal mixing on stratification and the ocean overturning circulation. J Phys Oceanogr 45:2580–2597. https://doi.org/10.1175/JPO-D-15-0039.1

Mashayek A, Ferrari R, Merrifield S, Ledwell JR, St Laurent L, Garabato AN (2017) Topographic enhancement of vertical turbulent mixing in the Southern Ocean. Nat Commun 2017:8. https://doi.org/10.1038/ncomms14197

Moore CM, Mills MM, Arrigo KR, Berman-Frank I, Bopp L, Boyd PW, Galbraith ED, Geider RJ, Guieu C, Jaccard SL, Jickells TD, La Roche J, Lenton TM, Mahowald NM, Marañón E, Marinov I, Moore JK, Nakatsuka T, Oschlies A, Saito MA, Thingstad TF, Tsuda A, Ulloa O (2013) Processes and patterns of oceanic nutrient limitation. Nature Geosci 6(9):701–710. https://doi.org/10.1038/ngeo1765

Munk WH (1966) Abyssal recipes. Deep-Sea Res Oceanogr Abstr 13(4):707–730. https://doi.org/10.1016/0011-7471(66)90602-4

Munk W, Wunsch C (1998) Abyssal recipes II: energetics of tidal and wind mixing. Deep-Sea Res Part I Oceanogr Res Pap 45:1977–2010. https://doi.org/10.1016/S0967-0637(98)00070-3

Naveira Garabato AC, Polzin KL, King BA, Heywood KJ, Visbeck M (2004) Widespread intense turbulent mixing in the Southern Ocean. Science 303(5655):210–213. https://doi.org/10.1126/science.1090929

Naveira Garabato AC, Frajka-Williams EE, Spingys CP, Legg S, Polzin KL, Forryan A, Povl Abrahamsen E, Buckingham CE, Griffies SM, McPhail SD, Nicholls KW, Thomas LN, Meredith MP (2019) Rapid mixing and exchange of deep-ocean waters in an abyssal boundary current. Proc Natl Acad Sci USA 116:13233–13238. https://doi.org/10.1073/pnas.1904087116

Nikurashin M, Vallis G (2011) A theory of deep stratification and overturning circulation in the ocean. J Phys Oceanogr 41(3):485–502. https://doi.org/10.1175/2010JPO4529.1

Nikurashin M, Vallis G (2012) A theory of the interhemispheric meridional overturning circulation and associated stratification. J Phys Oceanogr 42(10):1652–1667. https://doi.org/10.1175/JPO-D-11-0189.1

Nikurashin M, Ferrari R (2013) Overturning circulation driven by breaking internal waves in the deep ocean. Geophys Res Lett 40:31333137. https://doi.org/10.1002/grl.50542

Olsen A, Lange N, Key RM, Tanhua T, Álvarez M, Becker S, Bittig HC, Carter BR, Cotrim da Cunha L, Feely RA, van Heuven S, Hoppema M, Ishii M, Jeansson E, Jones SD, Jutterström S, Karlsen MK, Kozyr A, Lauvset SK, Lo Monaco C, Murata A, Pérez FF, Pfeil B, Schirnick C, Steinfeldt R, Suzuki T, Telszewski M, Tilbrook B, Velo A, Wanninkhof R (2019) GLODAPv2.2019—an update of GLODAPv2. Earth Syst Sci Data 11(3):1437–1461. https://doi.org/10.5194/essd-11-1437-2019

Palter JB, Sarmiento JL, Gnanadesikan A, Simeon J, Slater RD (2010) Fueling export production: Nutrient return pathways from the deep ocean and their dependence on the Meridional Overturning Circulation. Biogeosciences 7:3549–3598. https://doi.org/10.5194/bg-7-3549-2010

Ruan X, Thompson AF, Flexas MM, Sprintall J (2017) Contribution of topographically generated submesoscale turbulence to Southern Ocean overturning. Nat Geosci 10:840–847. https://doi.org/10.1038/NGEO3053

Saenko OA, Merryfield WJ, Lee WG (2012) The combined effect of tidally and eddy-driven diapycnal mixing on the large-scale ocean circulation. J Phys Oceanogr 42(4):526–538. https://doi.org/10.1175/JPO-D-11-0122.1

Sarmiento JL, Gruber N, Brzezinski MA, Dunne JP (2004) High-latitude controls of thermocline nutrients and low latitude biological productivity. Nature 427(6969):56–60. https://doi.org/10.1038/nature02127

Sigman DM, Hain MP, Haug GH (2010) The polar ocean and glacial cycles in atmospheric CO2 concentration. Nature 466:47–55. https://doi.org/10.1038/nature09149

Silvester JM, Lenn YD, Polton JA, Rippeth TP, Maqueda MM (2014) Observations of a diapycnal shortcut to adiabatic upwelling of Antarctic Circumpolar Deep Water. Geophys Res Lett. https://doi.org/10.1002/2014GL061538

Sloyan BM, Rintoul SR (2001) Circulation, renewal, and modification of antarctic mode and intermediate water. J Phys Oceanogr 34:1005–1030. https://doi.org/10.1175/1520-0485(2001)031<1005:CRAMOA>2.0.CO;2

St. Laurent L, Naveira Garabato AC, Ledwell JR, Thurnherr AM, Toole JM, Watson AJ (2012) Turbulence and diapycnal mixing in drake passage. J Phys Oceanogr 42(12):2143–2152. https://doi.org/10.1175/JPO-D-12-027.1

Stewart AL, Ferrari R, Thompson AF (2014) On the importance of surface forcing in conceptual models of the deep ocean. J Phys Oceanogr 44(3):891–899. https://doi.org/10.1175/JPO-D-13-0206.1

Talley LD (2013) Closure of the global overturning circulation through the Indian, Pacific, and southern oceans. Oceanography 26(1):80–97. https://doi.org/10.5670/oceanog.2013.07

Talley LD, Feely RA, Sloyan BM, Wanninkhof R, Baringer MO, Bullister JL, Carlson CA, Doney SC, Fine RA, Firing E, Gruber N, Hansell DA, Ishii M, Johnson GC, Katsumata K, Key RM, Kramp M, Langdon C, Macdonald AM, Mathis JT, McDonagh EL, Mecking S, Millero FJ, Mordy CW, Nakano T, Sabine CL, Smethie WM, Swift JH, Tanhua T, Thurnherr AM, Warner MJ, Zhang J-Z (2016) Changes in Ocean heat, carbon content, and ventilation: a review of the first decade of go-ship global repeat

hydrography. Ann Rev Mar Sci 8(1):185–215. https://doi.org/10.1146/annurev-marine-052915-100829

Tamsitt V, Drake HF, Morrison AK, Talley LD, Dufour CO, Gray AR, Griffies SM, Mazloff MR, Sarmiento JL, Wang J, Weijer W (2017) Spiraling pathways of global deep waters to the surface of the Southern Ocean. Nat Commun 8:1. https://doi.org/10.1038/s41467-017-00197-0

Thompson AF, Gille ST, MacKinnon JA, Sprintall J (2007) Spatial and temporal patterns of small-scale mixing in Drake Passage. J Phys Oceanogr 37(3):572–592. https://doi.org/10.1175/JPO3021.1

Verdy A, Mazloff MR (2017) A data assimilating model for estimating Southern Ocean biogeochemistry. J Geophys Res Oceans 122(9):6968–6988. https://doi.org/10.1002/2016JC012650

Waterhouse AF, Mackinnon JA, Nash JD, Alford MH, Kunze E, Simmons HL, Polzin KL, Laurent LCS, Sun OM, Pinkel R, Talley LD, Whalen CB, Huussen TN, Carter GS, Fer I, Waterman S, Naveira Garabato AC, Sanford TB, Lee CM (2014) Global patterns of diapycnal mixing from measurements of the turbulent dissipation rate. J Phys Oceanogr 44:1854–1872. https://doi.org/10.1175/JPO-D-13-0104.1

Watson AJ, Naveira Garabato AC (2006) The role of Southern Ocean mixing and upwelling in glacial-interglacial atmospheric CO2 change. Tellus B Chem Phys Meteorol 58(1):73–87. https://doi.org/10.1111/j.1600-0889.2005.00167.x

Watson AJ, Ledwell JR, Messias MJ, King BA, Mackay N, Meredith MP, Mills B, Naveira Garabato AC (2013) Rapid cross-density ocean mixing at mid-depths in the Drake Passage measured by tracer release. Nature 501(7467):408–411. https://doi.org/10.1038/nature12432

Watson AJ, Vallis GK, Nikurashin M (2015) Southern Ocean buoyancy forcing of ocean ventilation and glacial atmospheric CO2. Nat Geosci. https://doi.org/10.1038/NGEO2538

Wolff GA, Billett DSM, Bett BJ, Holtvoeth J, FitzGeorge-Balfour T, Fisher EH, Cross I, Shannon R, Salter I, Boorman B, King NJ, Jamieson A, Chaillan F (2011) The effects of natural iron fertilisation on deep-sea ecology: the Crozet Plateau, southern Indian ocean. PLoS ONE 6:e20697. https://doi.org/10.1371/journal.pone.0020697

Wunsch C, Ferrari R (2004) Vertical mixing, energy, and the general circulation of the oceans. Annu Rev Fluid Mech. 36:281–314. https://doi.org/10.1146/annurev.fluid.36.050802.122121